

Efficient GW calculations on two-dimensional materials using accurate long wavelength limit of the screened potential

Filip A. Rasmussen and Kristian S. Thygesen
*Center for Atomic-scale Materials Design (CAMD),
 Department of Physics and Center for Nanostructured Graphene (CNG),
 Technical University of Denmark, DK-2800 Kongens Lyngby, Denmark*
 (Dated: July 3, 2022)

Calculating the quasiparticle (QP) band structure of two-dimensional (2D) materials within the GW self-energy approximation has proven to be a rather demanding computational task. The main reason is that the strong \mathbf{q} -dependence of the 2D dielectric function around $\mathbf{q} = \mathbf{0}$ calls for a much denser sampling of the Brillouin zone than is necessary for similar 3D solids. Here we use an analytical expression for the small \mathbf{q} -limit of the 2D response function to perform the BZ integral over the critical region around $\mathbf{q} = \mathbf{0}$. This drastically reduces the requirements on the \mathbf{q} -point mesh and implies a significant computational speed-up. For example, in the case of monolayer MoS_2 , convergence of the G_0W_0 band gap to within $\sim 0.1\text{ eV}$ is achieved with 12×12 \mathbf{q} -points rather than the 36×36 mesh required with standard techniques. We obtain a converged G_0W_0 -LDA band gap of MoS_2 of 2.44 eV which increases to 2.75 eV in GW_0 . The method also explicitly accounts for dielectric anisotropy and we therefore also test the method on the highly anisotropic material phosphorene, a 2D allotrope of black phosphorous, and well-converged results for the QP band gap for this material is also reported.

PACS numbers: 71.15.Dx, 71.15.Qe, 73.22.-f

I. INTRODUCTION

The past few years have witnessed an explosion in research on atomically thin two-dimensional (2D) materials. Of particular interest are the 2D semiconductors including the family of transition metal dichalcogenides, which have been found to exhibit a number of unique opto-electronic properties.^{1–7} Of fundamental importance for understanding and predicting the opto-electronic properties is the electronic band structure of the material. The GW method,^{8,9} introduced by Hedin¹⁰ in 1965 and first applied to real solids in an ab-initio framework by Hybertsen and Louie¹¹ and Godby, Sham, and Schlüter,¹² has become the “gold standard” for calculating quasi-particle (QP) band structures. Over the years its performance has been thoroughly established for bulk materials^{13–15} and more recently also for molecules.^{16–19} In comparison, critical assessments of the accuracy and numerical convergence of GW calculations for 2D materials are rather scarce.^{20–23} These studies have shown that (i) it is essential to use a truncated Coulomb interaction to avoid long range screening between periodically repeated layers which reduces the QP band gap, and (ii) when a truncated Coulomb interaction is used, the convergence of the GW calculation with respect to the number of \mathbf{k} -points becomes much slower than is the case for similar bulk systems.

The slow \mathbf{k} -point convergence of the GW band structure is directly related to the nature of electronic screening in 2D which is qualitatively different from the well known 3D case.^{24,25} Specifically, while the dielectric function, $\epsilon(\mathbf{q})$, of bulk semiconductors is approximately constant for small wave vectors, the dielectric function of a 2D semiconductor varies sharply as $\mathbf{q} \rightarrow \mathbf{0}$.^{20,21} As a

consequence, the number of \mathbf{q} -points required to obtain a proper sampling of the screened interaction $W(\mathbf{q})$ over the Brillouin zone (BZ) is much higher for the 2D material than what would be anticipated from the 3D case. For example, the band gap of bulk MoS_2 is converged to within $\sim 0.1\text{ eV}$ with an in-plane \mathbf{k} -point grid of 12×12 while the same accuracy for monolayer MoS_2 requires a grid of 36×36 when standard BZ sampling schemes are applied.

Here we show that the slow \mathbf{k} -point convergence of the GW self-energy in 2D materials can be alleviated by performing the BZ integral of $W(\mathbf{q})$ analytically in the critical region around $\mathbf{q} = \mathbf{0}$ where $\epsilon(\mathbf{q})$ varies most strongly. The analytical expression for $W(\mathbf{q})$ is obtained from a lowest order expansion in \mathbf{q} of the head, $\chi_{00}^0(\mathbf{q})$, and wings, $\chi_{0\mathbf{G}}^0(\mathbf{q})$, of the non-interacting density response function. This simple scheme reduces the required number of \mathbf{q} -points by an order of magnitude without loss of accuracy.

II. GW SELF-ENERGY IN 2D

We split the GW self-energy into the exchange and correlation part, respectively. The former does not present particular problems in 2D materials and is performed using a Wigner-Seitz truncated Coulomb interaction as described elsewhere.²⁶ In a planewave expansion the corre-

lation part of the self-energy takes the form²⁷

$$\begin{aligned} \langle n\mathbf{k}|\Sigma^c(\omega)|n'\mathbf{k}\rangle &= \frac{i}{2\pi V} \int_{\text{BZ}} d\mathbf{q} \sum_{\mathbf{G}\mathbf{G}'} \int_{-\infty}^{\infty} d\omega' \bar{W}_{\mathbf{G}\mathbf{G}'}(\mathbf{q}, \omega) \\ &\times \sum_m \frac{[\rho_{n,\mathbf{k}}^{m,\mathbf{k}+\mathbf{q}}(\mathbf{G})][\rho_{n',\mathbf{k}}^{m,\mathbf{k}+\mathbf{q}}(\mathbf{G}')]^*}{\omega + \omega' - \epsilon_{m\mathbf{k}+\mathbf{q}} - i\eta \text{sgn}(\epsilon_{m\mathbf{k}+\mathbf{q}} - \mu)}, \end{aligned} \quad (1)$$

where the pair densities are defined as $\rho_{n\mathbf{k}}^{m,\mathbf{k}+\mathbf{q}}(\mathbf{G}) = \langle n\mathbf{k}|e^{i(\mathbf{G}+\mathbf{q})\cdot\mathbf{r}}|m\mathbf{k}+\mathbf{q}\rangle$, μ is the chemical potential, and $\bar{W}_{\mathbf{G}\mathbf{G}'}(\mathbf{q}, \omega)$ is the dynamical part of the screened potential given by

$$\bar{W}_{\mathbf{G}\mathbf{G}'}(\mathbf{q}, \omega) = v_{\mathbf{G}}(\mathbf{q}) [\varepsilon_{\mathbf{G}\mathbf{G}'}^{-1}(\mathbf{q}, \omega) - \delta_{\mathbf{G}\mathbf{G}'}], \quad (2)$$

where $v_{\mathbf{G}}(\mathbf{q}) = 4\pi/|\mathbf{G} + \mathbf{q}|^2$ is the Coulomb interaction. In most implementations the BZ integral in Eq. (1) is evaluated numerically with a standard quadrature method using a regular \mathbf{q} -point grid matching the \mathbf{k} -point grid of the ground state DFT calculation. Since the screened potential, Eq. (2), diverges at $\mathbf{q} = \mathbf{0}$ this point is handled separately, so the integral may be written

$$\int_{\text{BZ}} d\mathbf{q} \mathcal{S}(\mathbf{q}, \omega) \rightarrow \frac{\Omega}{N_{\mathbf{q}}} \sum_{\mathbf{q}_n \neq \mathbf{0}} \mathcal{S}(\mathbf{q}_n, \omega) + \int_{\Omega_0} d\mathbf{q} \mathcal{S}(\mathbf{q}, \omega), \quad (3)$$

where $\mathcal{S}(\mathbf{q}, \omega)$ denotes the entire integrand, Ω is the volume of the BZ, $N_{\mathbf{q}}$ is the total number of \mathbf{q} -points in the grid and Ω_0 denotes a small region around $\mathbf{q} = \mathbf{0}$. We now focus on how to calculate the contribution to the integral around the special point $\mathbf{q} = \mathbf{0}$.

Within the random phase approximation (RPA) the dielectric matrix is given by

$$\varepsilon_{\mathbf{G}\mathbf{G}'}(\mathbf{q}, \omega) = \delta_{\mathbf{G}\mathbf{G}'} - v_{\mathbf{G}}(\mathbf{q}) \chi_{\mathbf{G}\mathbf{G}'}^0(\mathbf{q}, \omega), \quad (4)$$

valid for all systems that extend infinitely in all directions. For a solid with a finite band gap it can be shown that the head of the non-interacting response function $\chi_{\mathbf{0}\mathbf{0}}^0(\mathbf{q}, \omega) \propto q^2$.²⁸ Since $v_{\mathbf{0}}(\mathbf{q}) = 4\pi/q^2$ it follows that in 3D the head of the dielectric function $\varepsilon_{\mathbf{0}\mathbf{0}}(\mathbf{q}, \omega)$ converges to a finite value > 1 when $q \rightarrow 0$. Moreover, this value is typically a reasonable approximation to $\varepsilon_{\mathbf{0}\mathbf{0}}(\mathbf{q}, \omega)$ in a relatively large region around $\mathbf{q} = \mathbf{0}$. This means that in the BZ integration in Eq. (1) around the singular point $\mathbf{G} = \mathbf{G}' = \mathbf{q} = \mathbf{0}$ all factors, except $1/q^2$, can be assumed to be constant and the integral can be performed analytically over a sphere centred at $\mathbf{q} = \mathbf{0}$,¹¹ computed numerically²⁹ or using an expansion of $W(\mathbf{q})$ in spherical harmonics.³⁰ (For simplicity we have neglected local field effects in the above analysis, but accounting for these do not change the conclusions).

For *GW* calculations on 2D materials performed with periodic boundary conditions, the direct use of Eq. (1) leads to significant over-screening due to the interaction between the repeated images.²¹ One way of dealing with

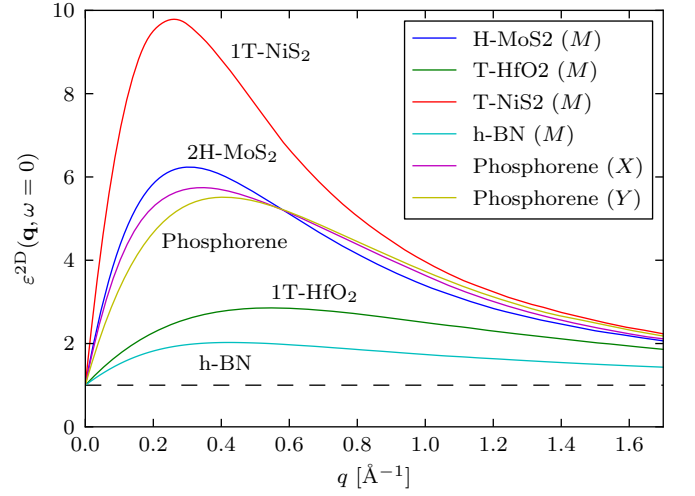


FIG. 1: (Color online) Static macroscopic dielectric function of a representative set of 2D semiconductors as a function of \mathbf{q} along the $\Gamma \rightarrow M$ direction for the hexagonal structures and along the path from Γ to X or Y in the case of phosphorene.

this is by subtracting the artificial contribution calculated from a classical electrostatic model.³¹ A more direct way of avoiding this unwanted interaction is to truncate the Coulomb interaction in the direction perpendicular to the layers. Thus in Eqs. (4) and (2), $v_{\mathbf{G}}(\mathbf{q})$ should be replaced by^{20,32}

$$v_{\mathbf{G}}^{2D}(\mathbf{q}) = \frac{4\pi}{|\mathbf{q} + \mathbf{G}|^2} \left[1 - e^{-|\mathbf{q}_{\parallel} + \mathbf{G}_{\parallel}|L/2} \cos(|G_z|L/2) \right], \quad (5)$$

where L is the length of the unit cell in the non-periodic direction. In the long wavelength limit $\mathbf{G} = \mathbf{0}$, $\mathbf{q} \rightarrow \mathbf{0}$, the truncated interaction becomes $v_{\mathbf{0}}^{2D}(\mathbf{q}) \approx \frac{2\pi L}{q}$ and the leading order of the head of the dielectric function thus becomes

$$\varepsilon_{\mathbf{0}\mathbf{0}}(\mathbf{q}) \approx 1 + \alpha q, \quad (6)$$

where we have assumed an isotropic material for simplicity (in general α will depend on the direction of \mathbf{q}).

Some examples of *macroscopic* dielectric functions for a representative set of 2D semiconductors are shown in Figure 1 (see Ref. 21 for a precise definition of this quantity). The linear form (6) is clearly observed in the small \mathbf{q} regime. Importantly, if we use the same strategy for evaluating the BZ integral in Eq. (1) as in 3D, i.e. approximating the integral by a mean value average on the discrete \mathbf{q} -point grid and replacing $\mathbf{q} = \mathbf{0}$ term of the bare Coulomb potential by its analytical integral over a small sphere, we obtain zero contribution for the $\mathbf{q} = \mathbf{0}$ term. This is because $\varepsilon_{\mathbf{0}\mathbf{0}}^{-1}(0) - 1 = 0$, see Eq. (2). On the other hand, by comparing Eqs. (6) and (2), and using the asymptotic form $v_{\mathbf{0}}^{2D}(\mathbf{q}) \approx \frac{2\pi L}{q}$ for the truncated Coulomb interaction, it follows that $\bar{W}_{\mathbf{0}\mathbf{0}}(\mathbf{q}) \approx 2\pi L\alpha/(1 + \alpha q)$ for small \mathbf{q} (assuming an isotropic material).

In Appendix A we show, following an analysis similar to that of Ref. 30, that for a general non-isotropic 2D material, the small \mathbf{q} limit of the head of the screened potential takes the form

$$\overline{W}_{00}(\mathbf{q}) = -2\pi L \frac{\hat{\mathbf{q}} \cdot \mathbf{A} \hat{\mathbf{q}}}{1 + |\mathbf{q}| \hat{\mathbf{q}} \cdot \mathbf{A} \hat{\mathbf{q}}}, \quad (7)$$

where $\hat{\mathbf{q}} = \mathbf{q}/|\mathbf{q}|$ and \mathbf{A} is a second rank tensor which also depends on the frequency. We see that we have exactly $\overline{W}_{00}(\mathbf{q} = \mathbf{0}) = -2\pi L \hat{\mathbf{q}} \cdot \mathbf{A} \hat{\mathbf{q}}$. The expression $\hat{\mathbf{q}} \cdot \mathbf{A} \hat{\mathbf{q}}$ is closely related to the slope of the dielectric function. In addition to Eq. (7) there are similar expressions for the wings and body of the screened interaction. When calculating the screened interaction at $\mathbf{q} = \mathbf{0}$ we use an average calculated by integrating these expressions in a small surrounding region numerically on a very fine grid (typically using an in-plane \mathbf{q} -point density of $6.25 \times 10^{-6} \text{ \AA}^2$).

A. Results

To investigate how this method performs we have carried out test calculations on the three monolayers h-BN, MoS₂ and phosphorene, which have quite different dielectric functions as seen on Figure 1. h-BN is a large gap dielectric with low screening ability leading to a small slope of the dielectric function at $\mathbf{q} = \mathbf{0}$, while MoS₂ has a larger dielectric function and quite steep slope at $\mathbf{q} = \mathbf{0}$. Phosphorene has a dielectric function similar to MoS₂ in size and steepness but is anisotropic with slopes varying by $\sim 40\%$ between the two high symmetry directions, $\Gamma \rightarrow X$ and $\Gamma \rightarrow Y$. For the present calculations we use for h-BN a lattice constant of 2.504 \AA and DFT calculations using PBE exchange-correlation (XC) functional. For MoS₂ we use an in-plane lattice constant of 3.184 \AA and a sulphur-sulphur distance of 3.127 \AA and the LDA XC functional. For phosphorene we use an in-plane unit cell of 4.611 \AA by 3.308 \AA , in-plane P-P-P angle of 95.9° , layer thickness of 2.114 \AA and the PBE XC functional. For all calculations the amount of surrounding vacuum has been such that the interlayer distance were in the range 10 to 15 \AA . The eigenvalues and wavefunctions obtained from the DFT calculations were used as input in the the *GW* calculation. The DFT calculations were done using a plane wave basis with a cut-off of 600 eV , while the dielectric function and the correlation self-energy were calculated using a much smaller basis size of either 50 eV (h-BN and MoS₂) or 75 eV (phosphorene). While this cut-off might not be enough to ensure properly converged quasi-particle energies, it is adequate to describe the trends related to the \mathbf{k} -point sampling relevant for this study.

In Figure 2 we compare the analytical small \mathbf{q} expression, Eq. (7), for the the head of the screened potential $\overline{W}_{00}(\mathbf{q})$ with the numerical values obtained using a fine and coarse \mathbf{k} -point sampling. In all the cases the $\mathbf{q} = \mathbf{0}$ value has been set to the analytical value. We notice that the screened potential falls off quickly and thus for

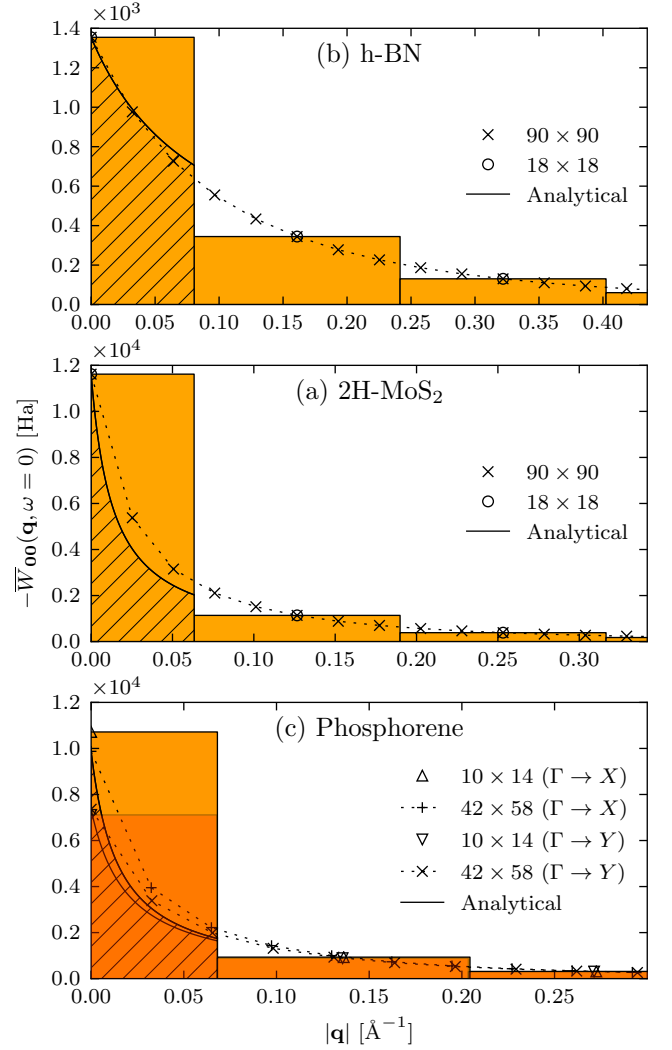


FIG. 2: (Color online) The head of the static component of the screened potential (subtracted the bare interaction) of monolayer a) h-BN b) MoS₂ and c) Phosphorene as a function of \mathbf{q} along the $\Gamma \rightarrow M$ direction or $\Gamma \rightarrow X$ and $\Gamma \rightarrow Y$ in the case of phosphorene. The crosses are the numerical values obtained on a fine \mathbf{q} -point grid while the circles or triangles represent the values obtained on a coarse \mathbf{q} -point grid. The dotted line is a linear interpolation of the numerically exact values. The bars represent a simple numerical approximation to the BZ integral of $\overline{W}_{00}(\mathbf{q})$ performed on the coarse \mathbf{q} -point grid. The value of the screened potential for $\mathbf{q} = \mathbf{0}$ is set to the analytical result Eq. (7). The full curve, shown only inside the $\mathbf{q} = \mathbf{0}$ bar, represents the analytical small \mathbf{q} approximation, Eq. (7), and the hatched area shows its contribution to the integral.

a coarse \mathbf{q} -point sampling the $\mathbf{q} = \mathbf{0}$ contribution to the integral is by far the largest and should therefore not be neglected. Similarly, just using the exact value in

$\mathbf{q} = \mathbf{0}$ could also pose a problem as the contribution will be grossly overestimated due to the convex nature of potential. Using the analytical limit within the region around $\mathbf{q} = \mathbf{0}$ however appears quite reasonable, although it clearly works better for h-BN than MoS₂ and phosphorene. We notice that the anisotropy of phosphorene makes $\bar{W}_{00}(\mathbf{q})$ non-analytical at $\mathbf{q} = \mathbf{0}$ (different limit values depending on the direction of \mathbf{q}). For larger \mathbf{q} the dielectric anisotropy becomes negligible; however, because of the relatively large weight of the $\mathbf{q} = \mathbf{0}$ contribution to the BZ integral, the anisotropy should be taken into account for accurate GW calculations.

We note that a similar approach to the treatment of the $\mathbf{q} = \mathbf{0}$ term of the screened potential was suggested in Ref. 20. That particular method was based on fitting to an empirical expression for $\varepsilon(q)$ calculated from the value at a small but finite \mathbf{q} . The method outlined here is different in that an analytical expression for $\bar{W}(\mathbf{q})$ obtained from a lowest order expansion of the head ($\chi_{00}^0(q)$) and wings ($\chi_{0\mathbf{G}}^0(q)$) of the non-interacting density response function³³ and thus can be obtained without fitting or using empirical parameters. This also ensures that the effect of in-plane dielectric anisotropy is explicitly included, which is seen to be quite significant for a material like phosphorene.

In Fig. 3 we show the correlation self-energy contribution to the G_0W_0 quasiparticle band gap of monolayer h-BN, MoS₂ and phosphorene as a function of $1/N_{\mathbf{k}}$ where $N_{\mathbf{k}}$ is the total number of \mathbf{k} -points in the BZ sampling (the \mathbf{q} point grid for the GW integration is the same as the \mathbf{k} -point grid used in DFT). We compare the results obtained using two methods: i) neglecting the $\mathbf{q} = \mathbf{0}$ contribution to head and wings of the screened potential and ii) evaluating Eq. (7) numerically on a fine grid in the $\mathbf{q} = \mathbf{0}$ region. It is clear that method i) in all cases underestimates the correlation self-energy due to the underestimation of the screening; in order to get the band gap converged to within ~ 0.1 eV one would have to use a \mathbf{k} -point sampling of minimum 30×30 for h-BN, 36×36 for MoS₂ and 22×30 for phosphorene. We also note that for large \mathbf{k} -point grids the band gaps using this method converge approximately as $1/N_{\mathbf{k}}$ as the missing contribution is almost proportional to the area of the $\mathbf{q} = \mathbf{0}$ region. Clearly, the latter approach varies significantly less with the \mathbf{k} -point grid and in fact the gap is converged to within 0.2 eV already for a \mathbf{k} -point grid in the order of 6×6 and to within ~ 0.1 eV with a 12×12 grid (in the worst case). We have performed test calculations for other 2D semiconductors and obtained similar conclusions although the number of \mathbf{k} -points required to reach convergence within 0.1 eV following the conventional approach ($\mathbf{q} = \mathbf{0}$ term neglected) is somewhat system dependent; materials with efficient screening, e.g. MoS₂ and NiS₂, require larger \mathbf{k} -point grids than materials with poor screening, e.g. h-BN and HfO₂ (see Fig. 1).

As mentioned, the self-energies shown in Fig. 3 were obtained with a rather low (50 eV to 75 eV) plane wave cut-off and may not be fully converged. In Table I we

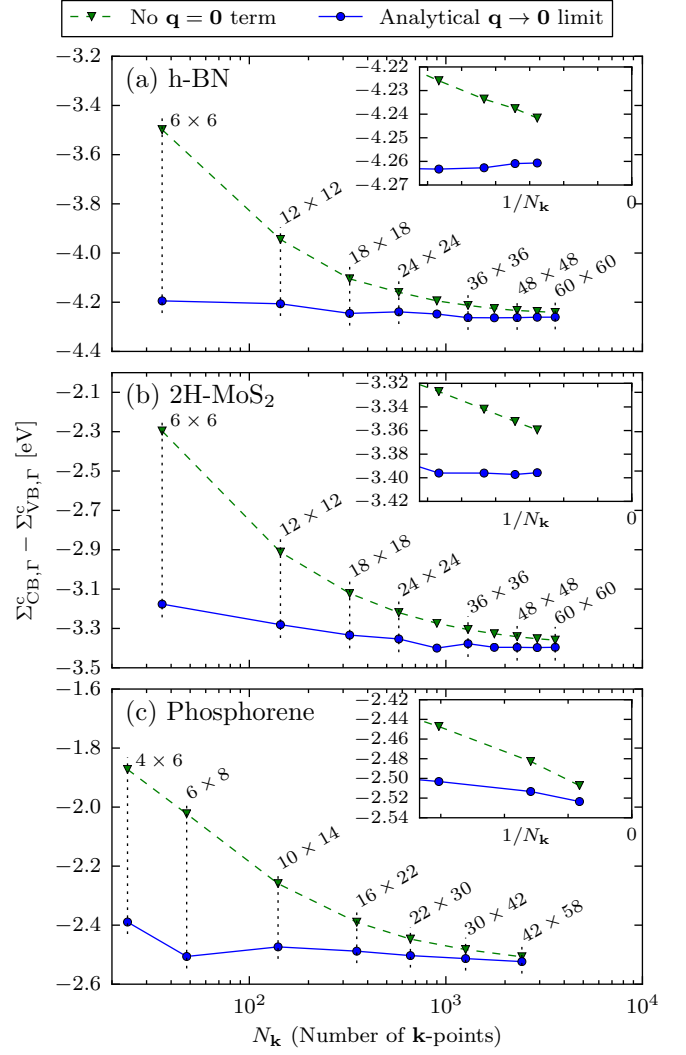


FIG. 3: (Color online) The correlation self-energy contribution to the G_0W_0 quasi-particle band gap of monolayer (a) 2H-MoS₂ (b) h-BN and (c) phosphorene, calculated using two different treatments of the $\mathbf{q} = \mathbf{0}$ term in Eq. (1). The dashed (green) line shows the contribution obtained when the head and wing elements of the $\mathbf{q} = \mathbf{0}$ term are neglected corresponding to the standard treatment used for 3D systems. The solid (blue) line shows the contribution obtained when using the analytical results, Eq. (7), to perform the integral over the $\mathbf{q} = \mathbf{0}$ element. The insets show the results for the largest \mathbf{k} -point grids on a reversed linear scale in $1/N_{\mathbf{k}}$.

report quasiparticle band gaps calculated by using self-energies obtained by a $1/N_{\text{pw}}$ extrapolation to the complete basis set limit using cut-off energies of up to 200 eV, which is needed to ensure proper convergence.^{34–36} For these calculations we used 12×12 \mathbf{k} -points for h-BN, 18×18 \mathbf{k} -points for MoS₂ and 10×14 for phosphorene with the analytical integration of $W(\mathbf{q})$ around $\mathbf{q} = \mathbf{0}$.

	DFT	G_0W_0	GW_0
h-BN (PBE)	4.54 eV	6.41 eV	6.91 eV
2H-MoS ₂ (LDA)	1.66 eV	2.44 eV	2.75 eV
2H-MoS ₂ (PBE)	1.66 eV	2.33 eV	-
Phosphorene (PBE)	0.89 eV	1.99 eV	2.23 eV

TABLE I: Direct band gaps calculated by DFT, G_0W_0 and GW_0 . The GW calculations were performed using analytic integration of $\bar{W}(\mathbf{q})$ around $\mathbf{q} = \mathbf{0}$ and the correlation self-energy has been extrapolated to an infinite basis set. Spin-orbit interactions were not included. The following \mathbf{k} -point grid were used; h-BN: 12×12 , 2H-MoS₂: 18×18 and phosphorene: 10×14 .

According to Fig. 3 this is sufficient to ensure convergence to within 0.1 eV. We note that spin-orbit interactions are not included in the reported values. Inclusion of spin-orbit interactions splits the valence band of MoS₂ at the K point by 0.15 eV thereby lowering the QP gap by around 0.07 eV.^{23,37} Our converged G_0W_0 @LDA band gap of 2.4 eV and G_0W_0 @PBE gap of 2.3 eV are both smaller than previously reported values of 2.5 eV to 2.8 eV.^{23,38} These have however been obtained without either a 2D truncation of the Coulomb potential or a proper treatment of the small \mathbf{q} screening in 2D and also suffered from insufficient size of the \mathbf{k} -point grids. An exception is Ref. 22 that reports a G_0W_0 @LDA band gap for MoS₂ of 2.70 eV using a truncated Coulomb interaction and a calculation of the screened potential at $\mathbf{q} = \mathbf{0}$ based on the method in Ref. 20. As of now we are not sure of the reason between the disagreement between that result and the ones reported here, but we note that in Ref. 22 they used a lattice constant of MoS₂ of 3.15 Å. This is 0.03 Å smaller than the one used for the calculations in this study and it is expected that the band gap increases with compressive strain,^{23,39} which could explain some of the difference. Our result of 2.4 eV is also smaller than the experimental value of 2.5 eV inferred from photo current spectroscopy.⁴⁰ However, performing partially self-consistent GW_0 the band gap increases to 2.75 eV (2.68 eV including spin-orbit), which is again larger than the experimental value. The method of Ref. 20 has also been used to calculate the G_0W_0 band gap of phosphorene where a value of 2.0 eV is reported,⁴¹ which is very close the value we obtain, despite the neglect of the dielectric anisotropy in the method used.

III. CONCLUSION

In conclusion, we have discussed the connection between the form of the \mathbf{q} -dependent dielectric function of a 2D semiconductor and the slow \mathbf{k} -point convergence of the GW band structure. We have derived an analytical expression for the $\mathbf{q} \rightarrow \mathbf{0}$ limit of the dynamical part of the screened potential of a semiconductor when a 2D truncation of the Coulomb potential is used.

This method also directly accounts for any dielectric anisotropy and does not rely on any additional parameters or fitting. Using this expression we have shown that convergence of the GW self-energy with respect to the size of the \mathbf{k} -point grid is drastically improved. For the specific case of monolayer MoS₂, we found that the use of the analytical form alone reduces the \mathbf{k} -point grid required to achieve convergence of the GW self-energy contribution to the band gap to within ~ 0.1 eV from around 36×36 to 12×12 – a reduction in the number of \mathbf{k} -points by a factor of ~ 9 . This method may therefore greatly aid in speeding up future calculations and open up the possibility of doing GW calculations for a broader range of 2D materials.

IV. ACKNOWLEDGEMENTS

We acknowledge support from the Danish Council for Independent Research's Sapere Aude Program, Grant No. 11-1051390. The Center for Nanostructured Graphene is sponsored by the Danish National Research Foundation, Project DNRF58.

Appendix A: Calculation of the $\mathbf{q} \rightarrow \mathbf{0}$ limit of the screened potential

In the following we derive the analytical form of the screened potential, Eq. (2), in the limit $\mathbf{q} \rightarrow \mathbf{0}$. We largely follow the approach of Ref. 30 where the same limit for bulk systems was considered. As explained in the main text we use a truncated Coulomb interaction of the form

$$v(\mathbf{r}_{\parallel}, z) = \frac{\theta(R - |z|)}{\sqrt{|\mathbf{r}_{\parallel}|^2 + z^2}}. \quad (\text{A1})$$

Using this potential we effectively turn off interaction between electrons on different 2D layers of the supercell calculation. We typically choose R to be half the height of the unitcell, $R = L/2$, so that an electron in the center of the layer will not interact with electrons located in the neighboring unitcell. In the following we will work with its Fourier transform given by

$$v_{\mathbf{G}}^{2D}(\mathbf{q}) = \frac{4\pi}{|\mathbf{q} + \mathbf{G}|^2} \left[1 - e^{-|\mathbf{q} + \mathbf{G}|L/2} \cos(|G_z|L/2) \right], \quad (\text{A2})$$

where \mathbf{q} is given in-plane only. We note that in the limit $L \rightarrow \infty$ it takes the usual 3D form, $v_{\mathbf{G}}(\mathbf{q}) = \frac{4\pi}{|\mathbf{q} + \mathbf{G}|^2}$. In the long wavelength limit it has the asymptotic behavior

$$v_0^{2D}(\mathbf{q}_{\parallel} \rightarrow \mathbf{0}) = \frac{2\pi L}{|\mathbf{q}|}, \quad (\text{A3})$$

diverging slower than the full Coulomb potential with profound consequences for the properties of 2D materials.

In the long wavelength limit $\mathbf{q} \rightarrow \mathbf{0}$ the non-interacting density response function or irreducible polarizability has the following behavior³³

$$\chi_{00'}^0(\mathbf{q} \rightarrow \mathbf{0}) = \mathbf{q} \cdot \mathbf{P}\mathbf{q} = |\mathbf{q}|^2 \hat{\mathbf{q}} \cdot \mathbf{P}\hat{\mathbf{q}} \quad (\text{A4})$$

$$\chi_{\mathbf{G}\mathbf{0}}^0(\mathbf{q} \rightarrow \mathbf{0}) = \mathbf{q} \cdot \mathbf{p}_{\mathbf{G}} = |\mathbf{q}| \hat{\mathbf{q}} \cdot \mathbf{p}_{\mathbf{G}}, \quad (\text{A5})$$

where \mathbf{P} is a second rank tensor, $\mathbf{p}_{\mathbf{G}}$ is a proper vector and $\hat{\mathbf{q}} = \mathbf{q}/|\mathbf{q}|$. The density response function, and therefore also \mathbf{P} and $\mathbf{p}_{\mathbf{G}}$, has a frequency dependence which here and through the rest of this section has been left out to simplify the notation. Within the random phase approximation the dielectric function is given by (schematically)

$$\varepsilon = 1 - v\chi^0. \quad (\text{A6})$$

Due to technical reasons^{13,42} it is easier to work with a similar symmetrized version given in Fourier space by

$$\tilde{\varepsilon}_{\mathbf{G}\mathbf{G}'}(\mathbf{q}) = \delta_{\mathbf{G}\mathbf{G}'} - \sqrt{v_{\mathbf{G}}(\mathbf{q})}\chi_{\mathbf{G}\mathbf{G}'}^0(\mathbf{q})\sqrt{v_{\mathbf{G}'}(\mathbf{q})}. \quad (\text{A7})$$

Inserting the Coulomb potential, Eq. (A2), and the expressions for the non-interacting response function Eqs. (A4)-(A5), the head and wings of the symmetrized dielectric function are

$$\begin{aligned} \tilde{\varepsilon}_{00}(\mathbf{q}_{\parallel} \rightarrow \mathbf{0}) &= 1 - \frac{2\pi L}{|\mathbf{q}|} |\mathbf{q}|^2 \hat{\mathbf{q}} \cdot \mathbf{P}\hat{\mathbf{q}} \\ &= 1 + |\mathbf{q}| \hat{\mathbf{q}} \cdot \mathbf{U}\hat{\mathbf{q}} \end{aligned} \quad (\text{A8})$$

$$\begin{aligned} \tilde{\varepsilon}_{\mathbf{G}\mathbf{0}}(\mathbf{q}_{\parallel} \rightarrow \mathbf{0}) &= -\sqrt{v_{\mathbf{G}}^{2D}(\mathbf{0})} |\mathbf{q}| \hat{\mathbf{q}} \cdot \mathbf{p}_{\mathbf{G}} \sqrt{\frac{2\pi L}{|\mathbf{q}|}} \\ &= \sqrt{|\mathbf{q}|} \hat{\mathbf{q}} \cdot \mathbf{u}_{\mathbf{G}} \end{aligned} \quad (\text{A9})$$

with $\mathbf{U} = -2\pi L\mathbf{P}$ and $\mathbf{u}_{\mathbf{G}} = -\sqrt{2\pi L v_{\mathbf{G}}^{2D}(\mathbf{0})} \mathbf{p}_{\mathbf{G}}$.

To determine the inverse dielectric function we write the dielectric function as a block matrix in the \mathbf{G}, \mathbf{G}' components with head, wings and body of the form

$$\tilde{\varepsilon} = \begin{pmatrix} H & \mathbf{w}^{\dagger} \\ \mathbf{w} & \mathbf{B} \end{pmatrix} \quad (\text{A10})$$

The inverse is then given by

$$\tilde{\varepsilon}^{-1} = \begin{pmatrix} (H - \mathbf{w}^{\dagger} \mathbf{B}^{-1} \mathbf{w})^{-1} & -(H - \mathbf{w}^{\dagger} \mathbf{B}^{-1} \mathbf{w})^{-1} \mathbf{w}^{\dagger} \mathbf{B}^{-1} \\ -\mathbf{B}^{-1} \mathbf{w} (H - \mathbf{w}^{\dagger} \mathbf{B}^{-1} \mathbf{w})^{-1} & \mathbf{B}^{-1} + \mathbf{B}^{-1} \mathbf{w} (H - \mathbf{w}^{\dagger} \mathbf{B}^{-1} \mathbf{w})^{-1} \mathbf{w}^{\dagger} \mathbf{B}^{-1} \end{pmatrix} \quad (\text{A11})$$

From this we see that

$$\tilde{\varepsilon}_{00}^{-1} = \left[\tilde{\varepsilon}_{00} - \sum_{\mathbf{G}, \mathbf{G}' \neq \mathbf{0}} \tilde{\varepsilon}_{\mathbf{G}\mathbf{0}}^* B_{\mathbf{G}\mathbf{G}'}^{-1} \tilde{\varepsilon}_{\mathbf{G}\mathbf{0}} \right]^{-1} \quad (\text{A12})$$

$$\tilde{\varepsilon}_{\mathbf{G}\mathbf{0}}^{-1} = \tilde{\varepsilon}_{00}^{-1} \sum_{\mathbf{G}' \neq \mathbf{0}} B_{\mathbf{G}\mathbf{G}'}^{-1} \tilde{\varepsilon}_{\mathbf{G}'\mathbf{0}} \quad (\text{A13})$$

$$\tilde{\varepsilon}_{\mathbf{G}\mathbf{G}'}^{-1} = B_{\mathbf{G}\mathbf{G}'}^{-1} + \tilde{\varepsilon}_{00}^{-1} \left(\sum_{\mathbf{G}'' \neq \mathbf{0}} B_{\mathbf{G}\mathbf{G}''}^{-1} \tilde{\varepsilon}_{\mathbf{G}''\mathbf{0}} \right) \left(\sum_{\mathbf{G}''' \neq \mathbf{0}} \tilde{\varepsilon}_{\mathbf{G}'''\mathbf{0}}^* B_{\mathbf{G}'''\mathbf{G}'}^{-1} \right) \quad (\text{A14})$$

Introducing the vector $\mathbf{a}_{\mathbf{G}}$ and the tensor \mathbf{A} given by

$$\mathbf{a}_{\mathbf{G}} = \sum_{\mathbf{G}'} B_{\mathbf{G}\mathbf{G}'}^{-1} \mathbf{u}_{\mathbf{G}'} \quad (\text{A15})$$

$$\mathbf{A} = \mathbf{U} - \sum_{\mathbf{G} \neq \mathbf{0}} \mathbf{u}_{\mathbf{G}}^* \otimes \mathbf{a}_{\mathbf{G}}, \quad (\text{A16})$$

where \otimes denotes the tensor product, the long wavelength limit of the inverse dielectric function is seen to be given

by

$$\tilde{\varepsilon}_{00}^{-1}(\mathbf{q} \rightarrow \mathbf{0}) = \frac{1}{1 + |\mathbf{q}| \hat{\mathbf{q}} \cdot \mathbf{A} \hat{\mathbf{q}}} \quad (\text{A17})$$

$$\tilde{\varepsilon}_{\mathbf{G}\mathbf{0}}^{-1}(\mathbf{q} \rightarrow \mathbf{0}) = -\frac{\sqrt{|\mathbf{q}|} \hat{\mathbf{q}} \cdot \mathbf{a}_{\mathbf{G}}}{1 + |\mathbf{q}| \hat{\mathbf{q}} \cdot \mathbf{A} \hat{\mathbf{q}}} \quad (\text{A18})$$

$$\tilde{\varepsilon}_{\mathbf{G}\mathbf{G}'}^{-1}(\mathbf{q} \rightarrow \mathbf{0}) = B_{\mathbf{G}\mathbf{G}'}^{-1} + \frac{|\mathbf{q}| (\hat{\mathbf{q}} \cdot \mathbf{a}_{\mathbf{G}}) (\hat{\mathbf{q}} \cdot \mathbf{a}_{\mathbf{G}'}^*)}{1 + |\mathbf{q}| \hat{\mathbf{q}} \cdot \mathbf{A} \hat{\mathbf{q}}} \quad (\text{A19})$$

Inserting these expression in the equation for the screened potential, Eq. (2), we see that the head and

wings are given by

$$\begin{aligned}\overline{W}_{00}(\mathbf{q} \rightarrow \mathbf{0}) &= v_0^{2D}(\mathbf{q}) [\tilde{\varepsilon}_{00}^{-1}(\mathbf{q}) - 1] \\ &= 2\pi L \frac{-\hat{\mathbf{q}} \cdot \mathbf{A}\hat{\mathbf{q}}}{1 + |\mathbf{q}|\hat{\mathbf{q}} \cdot \mathbf{A}\hat{\mathbf{q}}}\end{aligned}\quad (\text{A20})$$

$$\begin{aligned}\overline{W}_{\mathbf{G}\mathbf{0}}(\mathbf{q} \rightarrow \mathbf{0}) &= \sqrt{v_{\mathbf{G}}^{2D}(\mathbf{0})\tilde{\varepsilon}_{\mathbf{G}\mathbf{0}}^{-1}(\mathbf{q})}\sqrt{v_0^{2D}(\mathbf{q})} \\ &= -\sqrt{2\pi L v_{\mathbf{G}}^{2D}(\mathbf{0})} \frac{\hat{\mathbf{q}} \cdot \mathbf{a}_{\mathbf{G}}}{1 + |\mathbf{q}|\hat{\mathbf{q}} \cdot \mathbf{A}\hat{\mathbf{q}}}.\end{aligned}\quad (\text{A21})$$

and the body also gets a correction and becomes

$$\begin{aligned}\overline{W}_{\mathbf{G}\mathbf{G}'}(\mathbf{q} \rightarrow \mathbf{0}) &= \sqrt{v_{\mathbf{G}}^{2D}(\mathbf{0})v_{\mathbf{G}'}^{2D}(\mathbf{0})} [\varepsilon_{\mathbf{G}\mathbf{G}'}^{-1}(\mathbf{q}) - \delta_{\mathbf{G}\mathbf{G}'}] \\ &= \sqrt{v_{\mathbf{G}}^{2D}(\mathbf{0})v_{\mathbf{G}'}^{2D}(\mathbf{0})} \left[B_{\mathbf{G}\mathbf{G}'}^{-1} - \delta_{\mathbf{G}\mathbf{G}'} \right. \\ &\quad \left. + \frac{|\mathbf{q}|(\hat{\mathbf{q}} \cdot \mathbf{a}_{\mathbf{G}})(\hat{\mathbf{q}} \cdot \mathbf{a}_{\mathbf{G}'})}{1 + |\mathbf{q}|\hat{\mathbf{q}} \cdot \mathbf{A}\hat{\mathbf{q}}} \right].\end{aligned}\quad (\text{A22})$$

-
- ¹ K. F. Mak, C. Lee, J. Hone, J. Shan, and T. F. Heinz, Phys. Rev. Lett. **105**, 136805 (2010).
 - ² A. Splendiani, L. Sun, Y. Zhang, T. Li, J. Kim, C.-Y. Chim, G. Galli, and F. Wang, Nano Lett. **10**, 1271 (2010).
 - ³ H. Zeng, G.-B. Liu, J. Dai, Y. Yan, B. Zhu, R. He, L. Xie, S. Xu, X. Chen, W. Yao, and X. Cui, Sci Rep **3** (2013), 10.1038/srep01608.
 - ⁴ C. Zhang, A. Johnson, C.-L. Hsu, L.-J. Li, and C.-K. Shih, Nano Lett. **14**, 2443 (2014).
 - ⁵ Q. H. Wang, K. Kalantar-Zadeh, A. Kis, J. N. Coleman, and M. S. Strano, Nature Nanotechnology **7**, 699 (2012).
 - ⁶ L. Britnell, R. M. Ribeiro, A. Eckmann, R. Jalil, B. D. Belle, A. Mishchenko, Y.-J. Kim, R. V. Gorbachev, T. Georgiou, S. V. Morozov, A. N. Grigorenko, A. K. Geim, C. Casiraghi, A. H. C. Neto, and K. S. Novoselov, Science **340**, 1311 (2013).
 - ⁷ M. Bernardi, M. Palummo, and J. C. Grossman, Nano Lett. **13**, 3664 (2013).
 - ⁸ W. G. Aulbur, L. Jönsson, and J. W. Wilkins, in *Solid State Physics*, Vol. Volume 54, edited by Henry Ehrenreich and Frans Spaepen (Academic Press, 1999) pp. 1–218.
 - ⁹ F. Aryasetiawan and O. Gunnarsson, Rep. Prog. Phys. **61**, 237 (1998).
 - ¹⁰ L. Hedin, Phys. Rev. **139**, A796 (1965).
 - ¹¹ M. S. Hybertsen and S. G. Louie, Phys. Rev. Lett. **55**, 1418 (1985).
 - ¹² R. W. Godby, M. Schlüter, and L. J. Sham, Phys. Rev. Lett. **56**, 2415 (1986).
 - ¹³ M. Shishkin and G. Kresse, Phys. Rev. B **74**, 035101 (2006).
 - ¹⁴ T. Kotani and M. van Schilfgaarde, Solid State Communications **121**, 461 (2002).
 - ¹⁵ A. Marini, C. Hogan, M. Grüning, and D. Varsano, Computer Physics Communications **180**, 1392 (2009).
 - ¹⁶ C. Rostgaard, K. W. Jacobsen, and K. S. Thygesen, Phys. Rev. B **81**, 085103 (2010).
 - ¹⁷ F. Caruso, P. Rinke, X. Ren, A. Rubio, and M. Scheffler, Phys. Rev. B **88**, 075105 (2013).
 - ¹⁸ F. Bruneval, Phys. Rev. Lett. **103**, 176403 (2009).
 - ¹⁹ X. Blase, C. Attaccalite, and V. Olevano, Phys. Rev. B **83**, 115103 (2011).
 - ²⁰ S. Ismail-Beigi, Phys. Rev. B **73**, 233103 (2006).
 - ²¹ F. Huser, T. Olsen, and K. S. Thygesen, Phys. Rev. B **88**, 245309 (2013).
 - ²² D. Y. Qiu, F. H. da Jornada, and S. G. Louie, Phys. Rev. Lett. **115**, 119901 (2015).
 - ²³ F. A. Rasmussen and K. S. Thygesen, J. Phys. Chem. C **119**, 13169 (2015).
 - ²⁴ L. Keldysh, JETP Lett. **29**, 658 (1979), wOS:A1979JN00600015.
 - ²⁵ P. Cudazzo, I. V. Tokatly, and A. Rubio, Phys. Rev. B **84**, 085406 (2011).
 - ²⁶ R. Sundararaman and T. A. Arias, Phys. Rev. B **87**, 165122 (2013).
 - ²⁷ M. S. Hybertsen and S. G. Louie, Phys. Rev. B **34**, 5390 (1986).
 - ²⁸ R. M. Pick, M. H. Cohen, and R. M. Martin, Phys. Rev. B **1**, 910 (1970).
 - ²⁹ J. Deslippe, G. Samsonidze, D. A. Strubbe, M. Jain, M. L. Cohen, and S. G. Louie, Computer Physics Communications **183**, 1269 (2012).
 - ³⁰ C. Freysoldt, P. Eggert, P. Rinke, A. Schindlmayr, R. W. Godby, and M. Scheffler, Computer Physics Communications **176**, 1 (2007).
 - ³¹ C. Freysoldt, P. Eggert, P. Rinke, A. Schindlmayr, and M. Scheffler, Phys. Rev. B **77**, 235428 (2008).
 - ³² C. A. Rozzi, D. Varsano, A. Marini, E. K. U. Gross, and A. Rubio, Phys. Rev. B **73**, 205119 (2006).
 - ³³ J. Yan, J. J. Mortensen, K. W. Jacobsen, and K. S. Thygesen, Phys. Rev. B **83**, 245122 (2011).
 - ³⁴ M. L. Tiago, S. Ismail-Beigi, and S. G. Louie, Phys. Rev. B **69**, 125212 (2004).
 - ³⁵ B.-C. Shih, Y. Xue, P. Zhang, M. L. Cohen, and S. G. Louie, Phys. Rev. Lett. **105**, 146401 (2010).
 - ³⁶ J. Klimeš, M. Kaltak, and G. Kresse, Phys. Rev. B **90**, 075125 (2014).
 - ³⁷ Z. Y. Zhu, Y. C. Cheng, and U. Schwingenschlögl, Phys. Rev. B **84**, 153402 (2011).
 - ³⁸ A. Ramasubramanian, Phys. Rev. B **86**, 115409 (2012).
 - ³⁹ H. J. Conley, B. Wang, J. I. Ziegler, R. F. Haglund, S. T. Pantelides, and K. I. Bolotin, Nano Lett. **13**, 3626 (2013).
 - ⁴⁰ A. R. Klots, A. K. M. Newaz, B. Wang, D. Prasai, H. Krzyzanowska, J. Lin, D. Caudel, N. J. Ghimire, J. Yan, B. L. Ivanov, K. A. Velizhanin, A. Burger, D. G. Mandrus, N. H. Tolk, S. T. Pantelides, and K. I. Bolotin, Sci. Rep. **4** (2014), 10.1038/srep06608.
 - ⁴¹ V. Tran, R. Soklaski, Y. Liang, and L. Yang, Phys. Rev. B **89**, 235319 (2014).
 - ⁴² A. Baldereschi and E. Tosatti, Phys. Rev. B **17**, 4710 (1978).